Polymer Chain Conformation in the Melt during Steady Elongational Flow As Measured by SANS. Temporary Network Model

R. Muller,* C. Picot, Y. H. Zang, and D. Froelich

Institut Charles Sadron (CRM-EAHP), 4 rue Boussingault, 67000 Strasbourg, France.
Received September 6, 1989; Revised Manuscript Received November 1, 1989

ABSTRACT: The anisotropic form factor of a polymer sample with narrow molecular weight distribution was measured during simple elongational flow in the molten state. The strain rate range investigated corresponded to the linear viscoelastic regime for this polymer system, which allowed the experimental results to be checked in steady-state flow, and the reliability of the measurements to be assessed. It has been shown that a previously discussed relationship between tensile stress and recoverable strain allows the form factor of the chains to be calculated from only two physically meaningful parameters: the macroscopic recoverable strain and the number of submolecules between entanglements per chain. The agreement between the model and the experimental data is satisfactory in the molecular and submolecular scattering vector domain.

I. Introduction

Several previous investigations have shown that small-angle neutron scattering (SANS) can contribute valuable information about the dynamics of polymer networks or melts[1–4] with concurrent rheological measurements. Measurement of the anisotropic scattering correlation function $S(\tilde{q})$ of a strained polymer sample under an applied stress provides an efficient method of ascertaining chain conformation on a molecular level.

The traditional experimental method applied to polymer melts consists of uniaxially stretching a sample in the molten state containing deuterium-labeled chains and then freezing in the chain orientation by quenching below the glass transition temperature, T_G.[5] Scattering experiments are then performed at room temperature afterward. The main difficulty of this method arises from tricky experimental problems encountered in extensional rheometry of polymer melts.[6] In particular, the homogeneity of the sample deformation and of strain rate in the sample can be affected by gravity, temperature gradient, or inadequate clamping. Most available SANS data on melts relate to temperatures and strain rates corresponding to rubberlike behavior.[5,7]

In this study, we use a new extensional rheometer specifically designed to allow fast quenching of stretched specimens and for which special attention has been devoted to flow homogeneity and temperature control.[8] With such an apparatus, it was possible to perform the scattering experiments on elongated samples over a wide range of strain rates including the low strain rate range where the rheological behavior is linear viscoelastic.

In the present paper, we present experimental results that have been obtained for polystyrene samples with a narrow molecular weight distribution in the linear viscoelastic range of strain rate. This very simple situation demonstrates the reliability of the experimental method.

As will be seen, both the rheological behavior and the scattering correlation function can be accounted for within the framework of a temporary network model involving the recoverable strain of the specimen. The idea follows a previous rheological study[9] on a series of PS samples, showing that the true tensile stress in simple elongational flow can be formulated as a simple function of macroscopic recoverable strain. The results suggest a calculation of the scattering correlation function of a chain in an entangled melt similar to that of a multilinked chain in a cross-linked network using the samples' recoverable strain, instead of total strain, as the entanglement network deformation. The scattering of multilinked chains in elastomers has been examined by Ullman,[10] and the results of his calculations will be transposed directly to the case of melts.

II. Experimental Section

1. Experimental Device. All samples have been uniaxially stretched with the instrument schematically shown in Figure 1; a detailed description has been published elsewhere.[8] Its main features are the following: (a) symmetric stretching at constant strain rate with respect to the center of the specimen (this allows measurement of flow birefringence at a fixed point of the sample), (b) temperature control with a double silicone–oil bath, which can be removed by vertical displacement. This oven provides a good temperature control (less than ±0.2° gradient in the whole bath), whereas buoyancy prevents the specimen from flowing under the effect of gravity. Homogeneous deformation is thus achieved even at very low strain rates for which the time that the specimen stays in the molten state is longer than the terminal relaxation time of the polymer sample. Stretched specimens are quenched by rapid removal of the surrounding oil bath.

The linear viscoelastic data of the samples were determined with a Rheometrics RMS-605 rheometer in the oscillatory mode using parallel-disk geometry.

2. Samples. Two polystyrene samples having narrow molecular weight distributions were synthesized by anionic polymerization: one a hydrogenated polymer and the second a deuterated polymer with nearly the same molecular weight and distribution. Experimental details concerning the synthesis have been previously published.[11]

The weight-average molecular weight of the two samples was determined by light-scattering measurements in benzene taking into account the refractive index increments for PSH and PSD. The polydispersity was characterized by gel permeation chromatography using the universal calibration. The data are collected in Table I. It is seen that the weight- and z-average polymerization indices of the two polymers are very close.

0024-9297/90/2223-2577$02.50/0

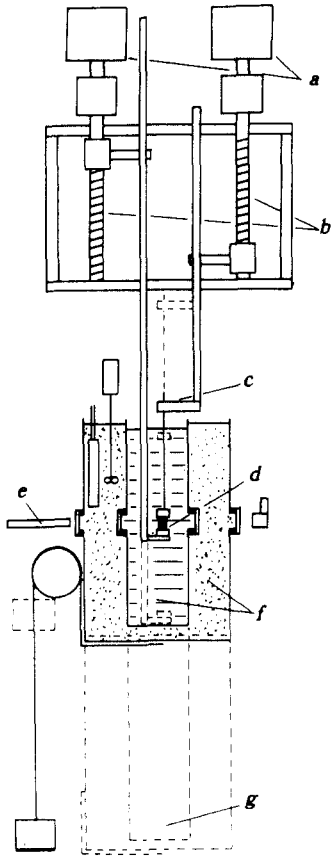

Figure 1. Schematic drawing of the extensional rheometer: (a) DC motors, (b) screws, (c) transducer, (d) specimen, (e) laser, (f) silicone-oil bath, (g) lower position of bath.

A mixture containing 10% by weight PSD and 90% by weight PSH was obtained from a (5% by weight) solution in benzene: The solution was thoroughly mixed for about 12 h, and the solvent was then removed by freeze-drying. To remove the last traces of benzene, which can play the role of a plasticizer in the rheological experiments, a further drying of the sample was carried out under vacuum at 70 °C for 3 days.

The specimens were molded at 160 °C under vacuum for about 30 min either in the form of disks (25 or 50 mm in diameter, 1.5 mm in thickness) for the oscillatory shear measurements or in the form of parallelepipeds (50 mm in length, 20 mm in width) for the extensional flow tests. The initial thickness of each specimen was chosen (between 1.2 and 2 mm) as a function of the final stretching ratio, so that the thickness of the stretched specimen in its final stage remained close to 1 mm. This is the optimal value for the SANS experiments, below which neutron absorption is less than 30% and for which no multiple scattering occurs.

III. Rheological Behavior

1. Dynamic Shear Measurements. The dynamic shear storage and loss moduli G' and G'' were measured as functions of frequency from 10^{-2} to 10^{2} rad·s^{-1} and at various temperatures from 120 to 180 °C. Two different transducers for the torque measurements and two sample diameters were used to obtain a good precision over the whole temperature domain. Small values of the strain amplitude were chosen, for which the rheological behavior was linear viscoelastic: typically 2% in the plateau zone and 10% in the terminal zone. Using time–temperature equivalence, master curves for G' and G'' are plotted: $G'(T_0\rho_0/T\rho)$ and $G''(T_0\rho_0/T\rho)$ vs ωa_T, T_0 being the reference temperature, a_T the thermal shift factor between T and T_0, and ρ the sample density. The temperature dependence of the thermal shift factor satisfies the WLF equation (T_G = 100 °C, c_1^g = 13.5, c_2^g = 50°). Figure 2 shows the master curves for G' and G'' when the temperature of the extensional tests (T_0 = 123 °C) was chosen as the reference temperature. The two viscoelastic constants of the terminal zone, zero shear viscosity and steady-state compliance, can be determined from these curves using the relationships

$$\eta_0 = \lim_{\omega\to 0} \frac{G''(\omega)}{\omega} \qquad J_e^0 = \lim_{\omega\to 0} \frac{G'(\omega)}{G''(\omega)^2} \tag{1}$$

The experimental values are $\eta_0 \simeq 3.8 \times 10^7$ Pa·s and $J_e^0 \simeq 10^{-5}$ Pa^{-1}.

2. Elongational Flow. All elongational tests have been carried out at constant elongational strain rate, $\dot{\epsilon}$ (which means exponentially increasing the stretching velocity of the sample between clamps).

Several experimental studies[8,12,13] have shown that time–temperature equivalence holds for elongational flow of polymer melts. For a constant strain rate experiment, the following equation holds

$$\eta_E^+(\dot{\epsilon},t,T_0) = \frac{\rho_0 T_0}{\rho T}\frac{1}{a_T}\eta_E^+(\dot{\epsilon}/a_T, ta_T, T) \tag{2}$$

where η_E^+ is the elongational stress–growth viscosity. This means that if the strain rate is varied over a wide enough range, the rheological behavior in elongational flow can be completely characterized at a single temperature.

In the present study, a temperature relatively close to T_G, T = 123 °C, was chosen with the intention of minimizing the relaxation of stress and chain orientation during the quenching: the weight-average relaxation time, λ_w, of the polymer melt at 123 °C can be calculated from the values of η_0 and J_e^0, $\lambda_w = \eta_0 J_e^0 \simeq 380$ s. On the other hand, cooling of the stretched specimen occurs by natural convection, and the actual cooling rate in the center of the stretched sample can be estimated for a typical final thickness of 1 mm: at 123 °C, the temperature decreases by 10° within a few seconds. Due to the strong temperature dependence of the thermal shift factor close to T_G, the time necessary for freezing the chain orientation will be of the same order, i.e., 100 times lower than λ_w.

For strain rates lower than 8×10^{-4} s^{-1}, it was found that the rheological behavior is nearly linear viscoelastic: Figure 3 shows the time-dependent elongational stress, $\sigma^+(\dot{\epsilon},t) = \dot{\epsilon}\eta_E^+(\dot{\epsilon},t)$, for three values of $\dot{\epsilon}$ (3.7×10^{-4}, 5.3×10^{-4}, and 7.4×10^{-4} s^{-1}); after about 1000 s, the stress reaches a steady value. For each strain rate, samples for the scattering experiments were obtained by quenching specimens at different macroscopic extensions in the steady-state flow as shown by the arrows in Figure 3. The recoverable strain was measured on all samples by cutting off a part of the stretched specimen (of initial length L_0) and annealing it at the surface of an oil bath at 150 °C for about 60 s. The recoverable strain was taken to be the quantity $(\lambda_r - 1)$ where $\lambda_r = L/L_0$, L being the length after recovery.

Comparison of $\sigma^+(\dot{\epsilon},t)$ for different samples stretched at the same strain rate shows that the reproducibility of the tests is satisfactory.

From the data in Table II it turns out that, for all samples, the steady-state elongational stress, σ, is almost equal to $3\eta_0\dot{\epsilon}$, where η_0 is the zero shear viscosity, whereas the quantity $(\lambda_r - 1)/\sigma$ remains close to the steady-state compliance. Both results are expected in the framework of

Table I
Molecular Weight Characteristics of Samples

sample	M_n	M_w	M_z	M_w/M_n	I_{Pn}	I_{Pw}	I_{Pz}	wt fractn in mixture
PSH	80 000	90 000	99 000	1.12	770	865	950	0.9
PSD	81 000	95 000	108 000	1.13	725	850	965	0.1

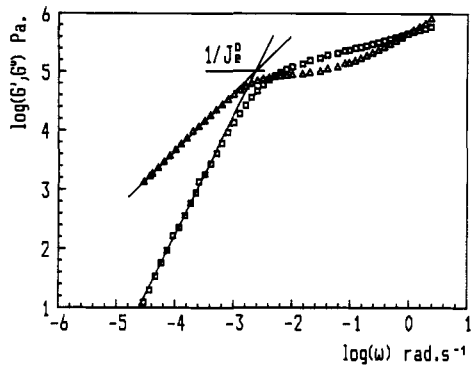

Figure 2. Master curves of $G'(\omega)$ (□) and $G''(\omega)$ (△) at T = 123 °C for the PSH/PSD mixture. Determination of J_e^0 from the behavior in the terminal zone (full lines).

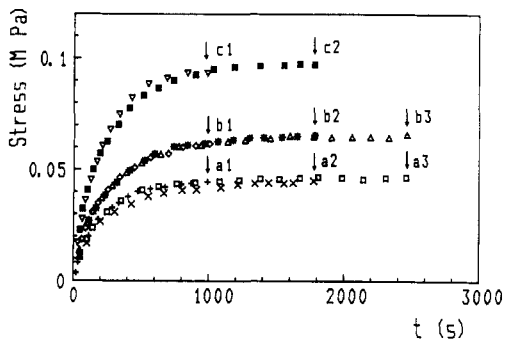

Figure 3. Stress–growth function in simple elongational flow at 123 °C. $\dot{\epsilon} = 3.7 \times 10^{-4}$ s^{-1}: a_1 (+), a_2 (×), a_3 (□); $\dot{\epsilon} = 5.3 \times 10^{-4}$ s^{-1}: b_1 (◇), b_2 (*), b_3 (△); $\dot{\epsilon} = 7.4 \times 10^{-4}$ s^{-1}: c_1 (▽), c_2 (■). Arrows indicate the time at which specimens have been quenched for the SANS experiments.

linear viscoelasticity. Since the experimental values of $\lambda_r - 1$ are noninfinitesimal, one might prefer to use the quantity $(\lambda_r^2 - \lambda_r^{-1})/3$ as a measure of the recoverable strain, by analogy with the expression of the Finger strain tensor in uniaxial extension. Actually, the two expressions do not differ by more than 3% at the highest strain rate.

IV. Small-Angle Neutron Scattering Results

The neutron scattering experiments were carried out at the Institute Laue Langevin, Grenoble, France, on two small-angle spectrometers in the following ranges of scattering vector amplitude: 4×10^{-3} Å$^{-1} < q < 3 \times 10^{-2}$ Å^{-1} (D11 spectrometer) and 10^{-2} Å$^{-1} < q < 1.2 \times 10^{-1}$ Å^{-1} (D17 spectrometer).

Water calibration[14] was used to convert the scattering data to an absolute coherent scattering cross-section, $S(\mathbf{q})$, with units of reciprocal centimeters. A general result for all samples of this study is the agreement between the data obtained on the two spectrometers in the overlapping q-domain (see Figures 5–7).

For a mixture of identically D-labeled chains in a matrix of H chains with the same polymerization index, $S(\mathbf{q})$ is given by

$$S(\mathbf{q}) = N\frac{\rho M}{m^2}(b_D - b_H)^2\varphi_D(1-\varphi_D)\,P(\mathbf{q}) = KM\varphi_D(1-\varphi_D)\,P(\mathbf{q}) \quad (3)$$

where b_D and b_H are the coherent scattering lengths of D and H monomer units, m and M are the molar weights of monomer unit and polymer chain, ρ is the density, φ_D is the volume fraction of labeled chains, N is Avogadro's number, and $P(\mathbf{q})$ is the form factor of the polymer chain.

1. Isotropic Sample. For an isotropic set of identical Gaussian coils, the form factor is given by the Debye function

$$g(q) = \frac{2}{x^2}(x - 1 + e^{-x}) \quad (4)$$

with $x = q^2R_g^2$, q the magnitude of the scattering vector $\mathbf{q}$, and R_g the radius of gyration of the chains. If a distribution of chain lengths is introduced, one obtains in the Guinier range

$$S(\mathbf{q})^{-1} = \frac{1}{K\varphi_D(1-\varphi_D)M_w}\left[1 + \frac{q^2}{3}\left(\frac{M_z b^2}{6m}\right)\right] \quad (5)$$

and in the intermediate q-range

$$q^2\,S(\mathbf{q}) = \frac{12K\varphi_D(1-\varphi_D)m}{b^2} \quad (6)$$

where b is the length of the monomer unit and M_w and M_z are the weight- and z-average of the molecular weight distribution.

The coherent scattering cross-section was measured for an isotropic sample molded as described in section I.2. For this sample, it has been checked that the scattering data are correctly correlated to the molecular weight distribution.

Experimentally, one finds from the Zimm plot (Figure 4) $(KM_w)^{-1} = 2.9 \times 10^{-3}$ cm (scattering cross-section at zero scattering vector) and $M_z b^2/6m = R_g^z = 82$ Å (z-average radius of gyration). The first value is in good agreement with the one (2.8×10^{-3} cm) calculated from M_w, m, ρ, b_D, and b_H. As seen in Figure 5, the experimental Kratky plateau is of the order of 0.115 cm^{-1} Å^{-2}, in close agreement with the value (0.12 cm^{-1} Å^{-2}) calculated according to eq 6, where b^2/m has been determined from R_g^z and M_z. Finally, our results (for the Kratky plateau and the molecular weight dependence of R_g^z) are in good agreement with other data published for PSD.[11,15]

Figure 5 shows the Kratky plot of the experimental data for the isotropic sample. In the calculated curve on the same figure, the form factor is the Debye function (eq 4) with $R_g = 82$ Å, and the Kratky plateau has been taken as 0.115 cm^{-1} Å^{-2}. With these values, the model of identical Gaussian chains fits the experimental data to a good approximation, which means that there is no need to consider molecular weight distribution effects in the interpretation of data for the anisotropic samples.

2. Oriented Samples. The anisotropic conformation of the chains in the oriented samples can be characterized by the form factor in the directions parallel and perpendicular to the stretching direction

$$P(\mathbf{q})^{\parallel} = \frac{1}{N^2}\sum_i\sum_j \langle \exp(iq^{\parallel}z_{ij})\rangle$$
$$P(\mathbf{q})^{\perp} = \frac{1}{N^2}\sum_i\sum_j \langle \exp(iq^{\perp}x_{ij})\rangle \quad (7)$$

where z is the stretching direction, x_{ij}, y_{ij}, and z_{ij} are the

Table II
Stress and Recoverable Strain for the Quenched Specimens

sample	$\dot{\epsilon}$, s^{-1}	time, s	stress, Pa	$\sigma/3\dot{\epsilon}$, MPa·s	recoverable strain	$(\lambda_r^2 - \lambda_r^{-1})/\sigma$, 10^{-6} Pa^{-1}
a_1	3.7×10^{-4}	1000	44 000	39	1.15	10.3
a_2	3.7×10^{-4}	1750	45 000	40	1.17	11.4
a_3	3.7×10^{-4}	2500	46 000	41	1.17	11.2
b_1	5.3×10^{-4}	1000	62 000	39	1.25	12.3
b_2	5.3×10^{-4}	1750	62 000	39	1.25	12.3
b_3	5.3×10^{-4}	2500	65 000	41	1.25	11.7
c_1	7.4×10^{-4}	1000	94 000	42	1.33	10.8
c_2	7.4×10^{-4}	1750	97 000	43	1.36	11.5

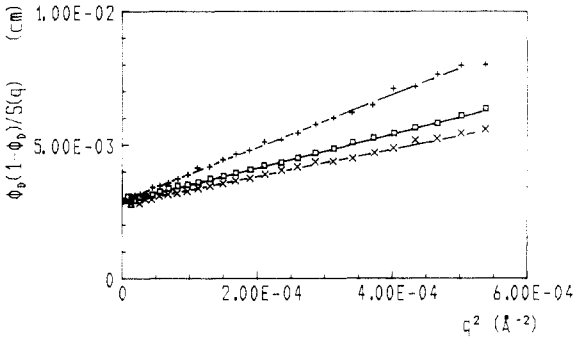

Figure 4. Zimm plot of the absolute coherent scattering cross-section reduced to the concentration of deuterated species: isotropic sample (□), c_1 in the parallel (+) and perpendicular (×) directions.

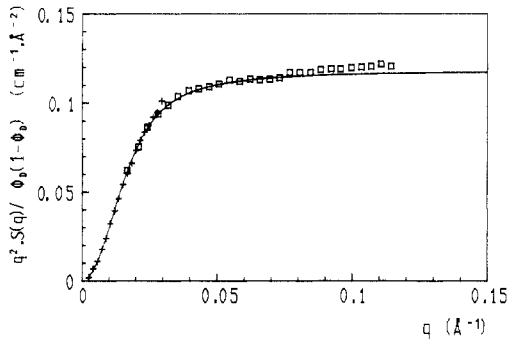

Figure 5. Absolute coherent scattering cross-section reduced to the concentration of deuterated species as a function of scattering vector in the Kratky representation for the isotropic sample. Experimental data from the D11 (+) and D17 (□) spectrometers. The full line is the Debye function for R_g = 82 Å.

components of the vector connecting monomer i to monomer j, and N is the number of monomer units per chain. $q^{\parallel}$ and $q^{\perp}$ are, respectively, the components of the scattering vector in the directions parallel and perpendicular to the stretching direction. Analysis of the scattering data has been carried out in radial sectors on the multidetector along both directions. For the samples of the present study the anisotropy is not very pronounced, and the scattering cross-sections $S(\mathbf{q})^{\parallel}$ and $S(\mathbf{q})^{\perp}$ are almost independent of the sector opening angle up to 30°.

Figure 6 shows the Kratky plots of the scattering cross-section in both directions for the three series of samples (a–c). From the Zimm plots in the Guinier range ($qR_g \ll 1$), it was possible to determine the parallel and perpendicular radii of gyration, $R_g^{\parallel}$ and $R_g^{\perp}$. In Figure 4, the Zimm plots for sample c_1 are shown as an example. The values for all samples are listed in Table III.

At this stage, several conclusions can be drawn on a qualitative level:

In steady elongational flow the anisotropic form factor becomes time-independent like the stress: The Kratky plots as well as the radii of gyration are the same for all samples of a given series (at constant strain rate but different macroscopic extensions). This result was actually expected; it confirms the reproducibility of the scattering measurements and more generally of the experimental method (stretching, quenching).

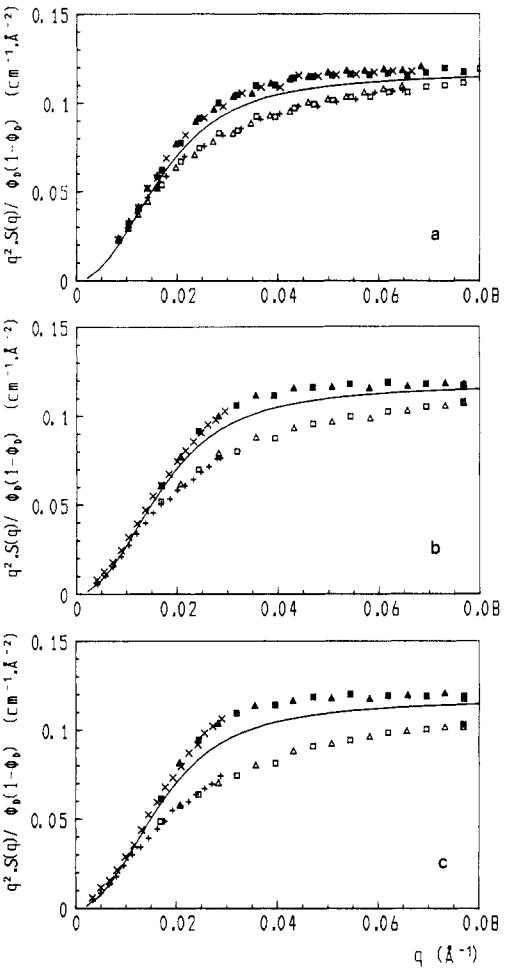

Figure 6. Same representation as in Figure 5 for the oriented samples. (a) Samples stretched at 3.7×10^{-4} s^{-1}; data from the D17 spectrometer in the parallel (+, □, △) and perpendicular (×, ■, ▲) directions; a_1 (+, ×), a_2 (□, ■), a_3 (△, ▲). (b) Samples stretched at 5.3×10^{-4} s^{-1}; data from the D11 (+, ×) and D17 (□, ■, △, ▲) spectrometers in the parallel (+, □, △) and perpendicular (×, ■, ▲) directions; b_2 (+, ×, □, ■), b_3 (△, ▲). (c) Samples stretched at 7.4×10^{-4} s^{-1}; data from the D11 (+, ×) and D17 (□, ■, △, ▲) spectrometers in the parallel (+, □, △) and perpendicular (×, ■, ▲) directions; c_1 (△, ▲), c_2 (+, ×, □, ■). The full line is the Debye function for R_g = 82 Å.

The anisotropy as measured by the gap between $q^2S(\mathbf{q})^{\parallel}$ and $q^2S(\mathbf{q})^{\perp}$ in the Kratky plots or by the increase of the parallel radius of gyration is indeed an increasing function of the strain rate.

In the perpendicular direction, there is little influence of the strain rate on the radius of gyration.

V. Temporary Network Model

1. Calculation of the Form Factor. Rheological models using the concept of a temporary network of entan-

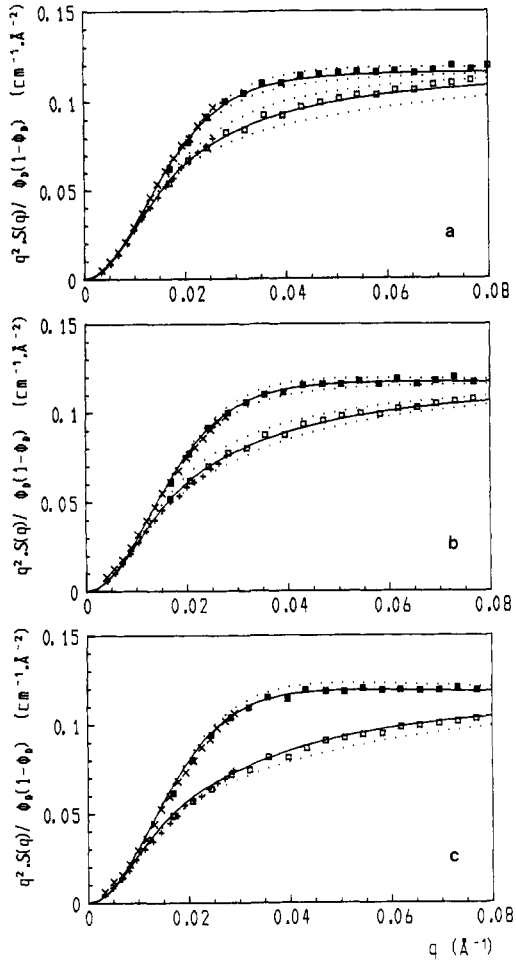

Figure 7. Data of Figure 6 compared with the form factor calculated from λ_r and n_e according to the temporary network model. (a) Influence of the number of submolecules for sample a_2 (λ_r = 1.17): (+, ×, □, ■) experimental data; inner dotted lines, n_e = 3; full lines, n_e = 5; outer dotted lines, n_e = 10. (b) Influence of network extension ratio for sample b_2 (n_e = 5): (+, ×, □, ■) experimental data; inner dotted lines, λ_r = 1.15; full lines, λ_r = 1.25; outer dotted lines, λ_r = 1.35. (c) Influence of assumption of dangling or fixed chain ends for sample c_2 (n_e = 5, λ_r = 1.36): (+, ×, □, ■) experimental data; full line, dangling end submolecules; dotted line, constrained end submolecules.

Table III
Radii of Gyration in Directions Parallel and Perpendicular to the Stretching Direction for Oriented Samples

	$R_g^{\parallel}$, Å		$R_g^{\perp}$, Å		$\frac{M}{\rho RT}\left(\frac{\sigma}{\lambda_r^2-\lambda_r^{-1}}\right)$
sample	exptl	calcd	exptl	calcd	
a_1	91.5	90.6	76.5	78.2	2.6
a_2	91	91.7	75.5	77.8	2.4
a_3	91	91.7	75.5	77.8	2.4
b_1	95.5	96.5	75	76.2	2.2
b_2	95.5	96.5	74.5	76.2	2.2
b_3	95	96.5	76.5	76.2	2.3
c_1	102	101.3	74.5	74.7	2.5
c_2	100.5	103.1	75.5	74.2	2.4

glements have been very successful in describing the rheological behavior of polymer melts[16] and especially the "strain-hardening" effect in elongational flow.[17] However, the assumption of affine displacement of temporary junctions with respect to macroscopic deformation leads in most cases to an overestimation of the stress.[18]

In a previous study[9] on un-cross-linked polystyrene melts, we discussed the following relation between the tensile stress in simple elongational flow and the recoverable strain, λ_r:

$$\sigma(\dot{\epsilon},t) = \sigma_v(\dot{\epsilon},t) + G(\dot{\epsilon})\,(\lambda_r^2 - \lambda_r^{-1}) \tag{8}$$

The first term on the right-hand side of eq 8 reaches a steady value at short times (typically for Hencky strains of the order of 0.5). Hence, the stress plotted as a function of the quantity $\lambda_r^2 - \lambda_r^{-1}$ leads to a straight line of slope $G(\dot{\epsilon})$. Experimentally, one finds that this slope increases with strain rate. For high enough strain rates, $G(\dot{\epsilon})$ is close to the plateau modulus, G_N^0 (2×10^5 Pa for polystyrene[19]). The idea of relating recoverable strain directly to the stress has been incorporated into a model proposed by Leonov.[20] This approach differs from that of the conventional temporary network (or a rubberlike liquid model) where the recoverable strain is found by solving an integral equation.[21]

By analogy with the well-known stress–strain relationship of the classical theory of rubber elasticity, one may assign the second term of the right-hand side of eq 8 to a Gaussian network with a number of moles, $\nu = G(\dot{\epsilon})/RT$, of elastic strands per unit volume and supporting a deformation that is exactly the macroscopic recoverable deformation. In the frame of the temporary network model, this means that (a) the effective deformation experienced by the entanglement network is the macroscopic recoverable deformation and (b) the number of effective entanglements per unit volume is, in general, a function of strain rate.

With respect to the scattering experiments, the above picture is of particular interest since it suggests that the calculated form factor of a labeled chain in an oriented entangled melt is the same as for a labeled path of identical length going through several covalent cross-links in a network stretched by an amount λ_r. The number of network strands to take into account on this path corresponds to the number of effective submolecules between entanglements on the chain, n_e. In these conditions, the relation between n_e and the shear modulus takes the form

$$n_e = \frac{M\nu}{\rho} = \frac{MG(\dot{\epsilon})}{\rho RT} \tag{9}$$

where M stands for the molecular weight of the chain and ρ is the density of the polymer. If $G(\dot{\epsilon}) = G_N^0$, n_e is equal to the ratio M/M_e, where M_e is the average molecular weight between entanglements determined from the plateau modulus (M_e = 18 000 g/mol).

The scattering of a labeled multi-cross-linked path in a strained network has been examined by Ullman.[10] This author has calculated the anisotropic form factor (eq 7) by assuming that all subchains between cross-links obey Gaussian statistics and have the same length. Chain ends are not connected to the network and are not constrained by the network deformation. The calculation needs to distinguish the various ways in which the pair of scattering units i and j can be distributed on the molecule (i and j on the same or on different end submolecules, i and j on the same or on different internal submolecules, or i on an end submolecule and j on an internal submolecule). Moreover, Ullman considered the general case (phantom network model) where the cross-links are allowed to fluctuate around mean positions affinely transformed in the macroscopic strain; the resulting scattering law therefore depends on network functionality, f.

In the present study, we assume that the junction points do not fluctuate, which amounts to taking f as infinite.

The numerical computation of $P(\mathbf{q})^{\parallel}$ and $P(\mathbf{q})^{\perp}$ involves the number, p, of scattering units per submolecule, the number, n_e, of submolecules per chain, the extension ratio, λ, of the entanglement network in the considered direction (λ_r or $\lambda_r^{-0.5}$), and the radius of gyration, R_g^0, of the chain in the undeformed state. The recoverable strain is known from experiment, p is related to n_e through the polymerization index of the chain ($p = I_P/n_e$), and n_e will be considered as an adjustable parameter, whose value is expected to lie around M/M_e.

The complete expression for $P(\mathbf{q}, p, n_e, \lambda, R_g^0)$ has been given by Bastide et al.[22] in the case of constrained end submolecules. These authors considered a path of high molecular weight containing about 50 submolecules, so that the contribution of dangling end submolecules could be neglected. This is not the case for the polymer melt of this study, for which the expected number of submolecules is of the order of $M/M_e \simeq 5$. The experimental data were therefore analyzed by writing out the expression of $P(\mathbf{q})^{\parallel}$ and $P(\mathbf{q})^{\perp}$ for unconstrained end submolecules.

2. Comparison with Experimental Results. For each strain rate (series a–c), we took the corresponding value of λ_r, known from experiment, and determined the number, n_e, of submolecules leading to the best agreement for $P(\mathbf{q})^{\parallel}$ and $P(\mathbf{q})^{\perp}$. The adjustment was carried out on the Kratky plots in the q-range (0.02–0.08 Å^{-1}). For the three series of samples, the best agreement is obtained for a value of n_e close to 5 as seen in Figure 7. Comparison of data and model in the Guinier range is readily performed on the parallel and perpendicular radii of gyration. According to the network model, one finds

$$R_g^{\parallel} = R_g^0\left[1 + (\lambda_r^2 - 1)\left(1 - \frac{1}{n_e} - \frac{7}{2n_e^2} + \frac{3}{n_e^3}\right)\right]^{0.5} \tag{10}$$

and a similar expression for $R_g^{\perp}$ by taking $\lambda_r^{-0.5}$ instead of λ_r. Table III shows that the experimental data for $R_g^{\parallel}$ and $R_g^{\perp}$ are in good agreement with eq 10 for the value of n_e (=5) adjusted from the Kratky plots (λ_r being taken as before as the experimental value).

It has to be mentioned that one can also determine a number of effective subunits between entanglements per polymer chain from the rheological data. If the equivalent shear modulus, $\sigma/(\lambda_r^2 - \lambda_r^{-1})$, determined from the experimental data for the stress and the recoverable strain is inserted in eq 9, a value close to 2.5 is obtained for all samples. Since no contribution to the stress arises from the dangling end submolecules, this value should be compared with $n_e - 2 = 3$, where n_e is the number of subunits determined from the scattering data.

Finally, we tested the sensitivity of the calculated form factor to the various parameters involved in the model. In the scattering range investigated ($q < 0.08$ Å^{-1}), the number, p, of scattering units per submolecule has almost no influence on the form factor as soon as the molecular weight of one scattering unit is taken to be lower than 200 g/mol. Figure 7a shows the influence of n_e, the number of subunits per chain, on $P(\mathbf{q})^{\parallel}$ and $P(\mathbf{q})^{\perp}$ at fixed value of λ_r. It appears that n_e can be determined with a relatively good precision from this type of measurement. The sensitivity of the calculated form factor to the extension ratio of the entanglement network is shown in Figure 7b, whereas Figure 7c compares the calculation with the assumption of dangling end submolecules and constrained end submolecules (for given values of n_e and λ_r). It appears that the difference cannot be neglected for small values of n_e.

VI. Conclusion

The aim of this study has been to establish a reliable relationship between the macroscopic deformation of a polymer melt and the molecular deformation as revealed by SANS. In the simple elongational flow geometry that has been investigated, the proposed model of a temporary network leads to a satisfactory description of the experimental results for $P(\mathbf{q})^{\parallel}$ and $P(\mathbf{q})^{\perp}$ both in the intermediate scattering vector range and in the Guinier range. When the assumption of dangling end subunits is used, the best agreement between the scattering data and the entanglement network model is obtained for a value of the average molecular weight between entanglements close to M_e ($\simeq$18 000 g/mol). The number of elastic strands per chain determined from stress and recoverable strain data leads to approximately the same value.

Our present data, restricted to the range of small strain rates, show that both the stress and the chain conformation are closely related to the macroscopic recoverable strain. The conventional rubberlike liquid model or the Doi–Edwards model would presumably do just as well in the range of linear viscoelasticity. The limitation of the proposed model has to be examined by carrying out experiments at higher strain rates and molecular weights. This will be the object of a future study, which should allow us to discriminate between the competing models.

Acknowledgment. We thank the Institute Laue Langevin (ILL, Grenoble, France) where neutron scattering experiments were carried out and especially our very efficient local contact A. Rennie. We are indebted to one of the reviewers for his pertinent comments. We also thank Prof. B. Bernstein and Dr. J. Klein for useful remarks on the manuscript.

References and Notes

(1) Picot, C. *Prog. Colloid Polym. Sci.* **1987**, *75*, 83.
(2) Boué, F. *Adv. Polym. Sci.* **1987**, *82*, 47.
(3) Boué, F.; Bastide, J.; Buzier, M.; Collette, C.; Lapp, A.; Herz, J. *Prog. Colloid Polym. Sci.* **1987**, *75*, 152.
(4) Bastide, J.; Buzier, M.; Boué, F. *Springer Proc. Phys.* **1987**, *29*, 112.
(5) Picot, C.; Duplessix, R.; Decker, D.; Benoit, H.; Boué, F.; Cotton, J. P.; Daoud, M.; Farnoux, B.; Jannink, G.; Nierlich, M.; de Vries A. J.; Pincus, P. *Macromolecules* **1977**, *10*, 437.
(6) Meissner, J. *Chem. Eng. Commun.* **1985**, *33*, 159.
(7) Boué, F.; Nierlich, M.; Jannink, G.; Ball, R. *J. Phys.* (*Les Ulis, Fr.*) **1982**, *43*, 137.
(8) Muller, R.; Froelich, D. *Polymer* **1985**, *26*, 1477.
(9) Muller, R.; Froelich, D.; Zang, Y. H. *J. Polym. Sci., Polym. Phys. Ed.* **1987**, *25*, 295.
(10) Ullman, R. *Macromolecules* **1982**, *15*, 1395.
(11) Cotton, J. P.; Decker, D.; Benoit, H.; Farnoux, B.; Higgins, J.; Jannink, G.; Ober, R.; Picot, C.; des Cloizeaux, J. *Macromolecules* **1974**, *7*, 863.
(12) Münstedt, H. *Rheol. Acta* **1975**, *14*, 1077.
(13) Münstedt, H.; Laun, H. M. *Rheol. Acta* **1979**, *18*, 492.
(14) Ullman, R. *Annu. Rev. Mater. Sci.* **1980**, *10*, 261.
(15) Wignall, G. D.; Bates, F. S. *J. Appl. Crystallogr.* **1987**, *20*, 28.
(16) Lodge, A. S.; Armstrong, R. C.; Wagner, M. H.; Winter, H. H. *Pure Appl. Chem.* **1982**, *54*, 1349.
(17) Wagner, M. H. *Rheol. Acta* **1979**, *18*, 33.
(18) Phan-Thien, N.; Tanner, R. I. *J. Non-Newtonian Fluid Mech.* **1977**, *2*, 353.
(19) Monfort, J. P.; Marin, G.; Monge, P. *Macromolecules* **1986**, *19*, 1979.
(20) Leonov, A. I. *Rheol. Acta* **1976**, *15*, 85.
(21) Wagner, M. H.; Stephenson, S. E. *J. Rheol.* **1979**, *23*, 489.
(22) Bastide, J.; Herz, J.; Boué, F. *J. Phys.* (*Les Ulis, Fr.*) **1985**, *46*, 1967.

Registry No. PS, 9003-53-6; neutron, 12586-31-1.